Impact of neutron irradiation on the strength and ductility of pure and ZrC reinforced tungsten grades

Chao Yin [a,b], Dmitry Terentyev [a], Tao Zhang [c], Roumen H. Petrov [d,e], Thomas Pardoen [b]

[a] Structural Materials Group, Institute of Nuclear Materials Science, SCK CEN, 2400 Mol, Belgium
[b] Institute of Mechanics, Materials and Civil Engineering, UCLouvain, 1348 Louvain-la-Neuve, Belgium
[c] Institute of Solid State Physics, Chinese Academy of Sciences, Hefei, Anhui 230031, China
[d] Department of Electrical Energy, Metals, Mechanical Constructions & Systems, Ghent University, 9052 Ghent, Belgium
[e] Department of Materials Science and Engineering, Delft University of Technology, Delft, 2082, The Netherlands

Corresponding author: Chao Yin
Email: cyin@sckcen.be

Abstract

The strength and ductility of two tungsten products, developed for application in nuclear fusion environment, are studied before and after neutron irradiation using uniaxial tensile tests. The first product is a commercially pure tungsten, produced by AT&M company according to ITER specification, and the second one is reinforced with zirconium carbide (W-ZrC) particles. The addition of ZrC particles leads to a reduction of the ductile to brittle transition temperature (DBTT) in non-irradiated conditions down to 50-100 ºC without loss of strength and of other attractive properties of tungsten.

The neutron irradiation was performed in the range 625-700 ºC up to 1.125 dpa. The tests were performed to screen the shift of the DBTT as well as to characterize the evolution of the strength and ductility at the irradiation temperature. In addition, a series of interrupted tensile tests were performed in order to determine the variation of the yield strength as a function of temperature using an original single specimen test method.

The neutron irradiation causes the reduction of the total elongation of both tungsten products. The DBTT range, which was evaluated from the tensile test results, of W-ZrC lies in the 300 to 500 ºC range (while it is ~100 ºC in non-irradiated state). The DBTT range of pure tungsten is between 400 to 575 ºC i.e. higher than that of W-ZrC. The irradiation hardening, measured at ~600 ºC, which is close to the irradiation temperature, leads to an increase of the proof stress by a factor of two in both studied grades. Despite that the irradiation induced hardening, both products retain a total elongation of about 10% prior to fracture. W-ZrC exhibits a similar total elongation at 500 ºC, thus maintaining a significant ductility resource, while pure W becomes brittle at 500 ºC and below.

Keywords: Tungsten, Neutron irradiation, Tensile test, Single specimen test, DBTT

1. Introduction

Tungsten is the main candidate material for the plasma facing components (PFCs) in the ITER divertor, DEMO divertor and DEMO blanket armor [1-4]. A significant part of the thermal energy from the nuclear fusion reaction will be extracted by stopping fast 14 MeV neutrons inside PFCs. The development of materials capable to withstand significant neutron fluences is one of the headline missions indicated in the Fusion Electricity Roadmap [5]. Neutron irradiation degrades thermal, physical and mechanical properties of materials thereby causing technological and safety concerns under prolonged operation [6].

Although tungsten (W) has a number of advantages compared to other metals such as a high melting point, a low erosion rate, a high thermal conductivity, and an excellent thermal stress resistance [7], the ductile to brittle transition temperature (DBTT) around 300-400 ^{o}C is unfortunately also rather high [8]. Coupled with the effect of neutron irradiation hardening, the irradiation-induced embrittlement might induce some severe limits on the operational conditions for the application of W as PFC [9-11]. This, in turn, might have an impact on the selection of coolant and period of PFC maintenance. This is why the investigation of neutron irradiation effects and the development of low-DBTT materials/composites is carried out in parallel.

The mechanical properties of the commercial tungsten in the non-irradiated state, produced by hot rolling/forging (e.g. produced by Plansee and ALMT companies), have been studied earlier in Refs. [12-17] including investigation of the effect of texture, annealing and cold-rolling processing. Overall, it is agreed that the successful application of W in fusion reactors will be determined by the best compromise between a reduced DBTT and an enhanced fracture toughness as well as a high recrystallization temperature. For that purpose, advanced W-based grades are under development to improve low- and high-temperature performance. For instance, particle-reinforced tungsten and reduced grain size material can suppress grain growth, improve the strength of grain boundaries as well as the fracture toughness, and reduce the DBTT (see reviews [18, 19]). By using dedicated alloying with zirconium carbide (ZrC) nano-sized particles in a powder metallurgy-based process, it was possible to reduce the free oxygen occupying grain boundaries and successfully fabricate bulk plate of W-0.5 wt.% ZrC alloy [20]. Preliminary mechanical and high heat flux (HHF) assessment demonstrated that this material exhibits a DBTT as low as 100 ^{o}C and sufficiently withstands HHF loads up to a power density of 0.66 GW/m^2 [20], simulated by the electron beam. Our recent work [21] was dedicated to the comparison of several commercial and lab-scale W products in terms of tensile properties in the temperature range where the irradiation hardening is expected to be the limiting factor. Among a number of tested products, tungsten-zirconium carbide alloy (W-0.5ZrC) was found to involve the lowest DBTT (around 100 ^{o}C), as indicated in the original work [20] while still maintaining a rather high yield strength. The next step is thus to investigate the impact of neutron damage on this perspective tungsten grade.

The information about the impact of neutron irradiation on the mechanical properties of tungsten is rather scarce. Back to 1979, Alexandrov and Gorynin [11] studied the tensile properties of sintered pure W irradiated at 100 ^{o}C up to a dose of 4.2 x 10^{19} n/cm^2 (about 0.05 dpa) and showed that the DBTT shifted from 400 to ~600 ^{o}C, while the ultimate tensile strength (UTS) increased nearly by a factor of two (from ~500 MPa to ~900 MPa for test temperature at 500 ^{o}C and ~400 MPa to ~600 MPa for test temperature at 800 ^{o}C). The irradiation of sintered W at 371-380 ^{o}C to 0.5-0.9 x 10^{22} n/cm^2 (i.e. 0.5-0.9 dpa) revealed similar behavior i.e. the increase of the strength (factor of 2) and a decrease of the ductility with a DBTT shift of about 300-350 ^{o}C [9]. Gorynin et al. [10] studied the mechanical properties of tungsten under neutron irradiation up to 2.2 x 10^{22} n/cm^2 (i.e. > 2.5 dpa) at 350, 500 and 800 ^{o}C on fast-type BOR60 reactor and measured the tensile properties. The general conclusion was that under irradiation at 350 and 500 ^{o}C, tungsten exhibits brittle fracture, while at 800 ^{o}C the material remains ductile at the irradiation temperature. Recently, tensile tests of single crystal tungsten samples after irradiation to 0.4 dpa at 690-800 ^{o}C were performed in [22]. Whereas unirradiated samples exhibited ductility starting at 300 ºC, this shifted to above 500 ºC after irradiation [23]. Three point bending tests on tungsten specimens (irradiated on the spallation neutron source) were performed by Habainy et al. [24]. The samples were irradiated by high-energy protons and spallation neutrons at temperatures up to 500 ºC and damage up to 3.5 dpa. Whereas DBTT of unirradiated specimens was around 350 ºC, all irradiated specimens exhibited brittle fracture at test temperatures up to 500 ºC. Based on this literature review, one can conclude that neutron irradiation performed in the 400-800 ºC temperature range with a dose varying between 0.5 and 2 dpa leads to the embrittlement of tungsten with a transition temperature around 500 to 600 ºC, depending on the irradiation temperature and fluence. Therefore, it is critical to understand the impact of neutron irradiation on the mechanical properties of tungsten in this temperature range.

The present work is dedicated to the systematic characterization of the strength and tensile ductility before and after neutron irradiation of commercially pure W grade, produced according to ITER specifications, and W-ZrC alloy, which is known to have very low DBTT [20, 25, 26]. Neutron irradiation is performed in the BR2 reactor, Belgium, at 600-800 ºC up to a dose of ~ 0.8-1 dpa. The purpose of this study is to extend the exploration of irradiation induced embrittlement in pure W with ITER specification and to compare it with the low-DBTT W-ZrC grade. An additional interesting result of this work is the development of a single specimen test method for the determination of the strength-temperature relationship in order to limit the number of irradiated material samples required to identify the DBTT threshold.

2. Experimental

The experimental section consists of three parts, namely: a brief description of the test materials (detailed information could be found in earlier works [21, 27]), a description of the irradiation device and tensile test procedures. The latter contains a description of the standard and interrupted uniaxial tensile tests which we applied here to deduce the yield strength to generate the maximum amount of information with one specimen. The procedure does not follow the currently available standards and therefore we provide a detailed description in Annex A together with examples of the application of this original test procedure on tungsten and ferritic martensitic steel.

2.1. Materials

One commercial tungsten product fabricated according to ITER specification (referred to as ATW, which is the abbreviation of AT&M tungsten) is compared to one lab-scale tungsten product (referred to as WZrC, with the zirconium-carbide strengthening applied in this product). ATW is a rolled pure tungsten plate of 13 mm thickness produced by AT&M China with a medium equivalent grain size of ~60 µm [21]. WZrC is a rolled tungsten (formed as a plate of 8 mm thickness) reinforced with 0.5 wt% of ZrC produced by the Institute of Solid State Physics, Chinese Academy of Science with a medium equivalent grain size of ~7 µm [21]. The medium equivalent grain size is defined as the equivalent diameter of grains corresponding to 50% cumulative area fraction. Although both products are rolled after sintering, WZrC was processed following a thermal mechanical treatment (TMT) to reduce grain size and have nearly equiaxed grains [20, 21]. The uniaxial tensile specimens are machined along the rolling direction (RD) also called longitudinal direction (LD). Therefore, the specimens are named with the indication of sampling direction: ATW-L and WZrC-L. The inverse pole figure of both products and specimen dimensions are shown in Fig. 1 where TD is the abbreviation of transverse direction. For a comprehensive analysis of the interrupted test method proposed in this study, RAFM steel (referred to as Eurofer97) of Eurofer97 specification [27] is used to conduct tests in the non-irradiated condition. The chemical composition and production route is within the specification of the Eurofer97 steel.

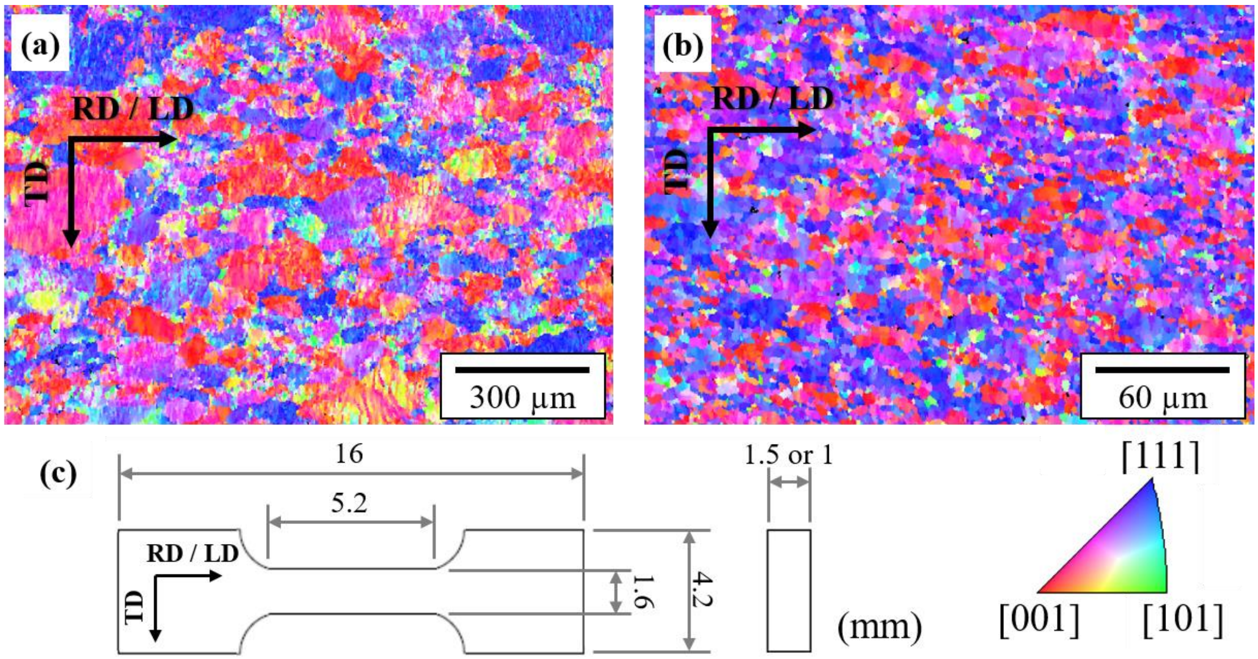

Fig. 1. Normal direction inverse pole figure of (a) ATW and (b) WZrC. (c) Schematic of the tensile specimen with dimensions [21] (the thicknesses of specimen for tungsten and Eurofer97 are 1.5 mm and 1 mm, respectively).

2.2. Neutron irradiation

Neutron irradiation was performed in the Belgian Material Test Reactor BR2. The specially developed irradiation device (rig) was used to deliver fusion-relevant irradiation conditions. In particular, the rig was actively cooled with helium gas and the temperature on the samples was measured at several positions of the rig. The rig itself is made of a 1.5 mm thick stainless steel pressurized pipe, which is plugged to an out of pile equipment controlling temperature by adjusting the gas pressure. The temperature is monitored with four thermocouples located in different parts of the rig. The central part of the rig exhibits a flat temperature profile set to be 800 ºC. To avoid "cold start", the rig was equipped with an electrical heater, which enables the heating of the samples up to 800 ºC before the irradiation starts.

The rig was designed to deliver ~50% of the volume with active temperature control (i.e. central part of the rig) while outer regions would exhibit a temperature gradient due to the reduction of the neutron flux. The temperature at the ends of the rig was 550 ºC. Such design not just allows for extremely accurate temperature control in the central part (±3 ºC) but also exhibits reasonable temperature oscillations in the outer parts. For the samples studied in this work, the temperature fluctuation was ±20 ºC.

The rig was placed directly inside the fuel element in the position close to the central channel of the reactor such that in a mid-plane the fast neutron (E > 0.1 MeV) flux is equal to 7×10^{14} n/cm^2/s at a nominal power of 60 MW.

The samples were fixed inside the graphite matrix, which was machined to accommodate the samples, heater, and feedthrough for thermocouples. In order to avoid carbon contamination, the samples were wrapped in the 25 µm tungsten foil. The graphite holder consists of 26 units, where each unit has a height of 27 mm and could accommodate either 8 tensile test specimens or 4 fracture toughness specimens (of KLST type). The example of the irradiation temperature profile during one cycle (28 days) on the specimens located in the T-controlled and outer regions is provided in Fig. 2. In addition to the thermocouple data, the reactor power is added to the figure. Due to the parallel irradiation experiment, the reactor power was reduced by ~10%, and one can see that this power reduction did not have any impact on the stability of the irradiation temperature, practically. The graphite matrix consists of 26-unit sample holders (13 and 14 holders were located exactly in the mid-flux position). The samples studied here were extracted from the unit holders 5, 7, 8, which have a mean irradiation temperature of 625 ºC, 680 ºC, and 700 ºC, respectively.

The irradiation was performed for 6 cycles in order to accumulate 1.25 dpa (in W) in the central part of the rig. The irradiation dose of 0.975, 1.075 and 1.125 dpa was imposed, respectively, in the holders 5, 7, and 8.

The irradiation dose was calculated by MCNPX 2.7.0 [28]. The dpa cross sections for W have been prepared from the JENDL4 file (MT444) for the threshold displacement energy of 55 eV, following the recommendation of IAEA [29]. The transmutation of Re and Os was calculated based on the ALEPH code developed by SCK CEN and available nuclear databases [30-34]. The transmutation of tungsten resulted in the production of 1.5 at% Re and 0.2 at% Os on the samples irradiated up to 1.125 dpa. The samples at lower irradiated doses exhibit lower concentrations of Re and Os. Note that the established levels of Re and Os are much lower than what was typically reported in other irradiation studies performed e.g. at the HFIR reactor, which has a similar neutron spectrum. In the current experiment, the strong reduction of the transmutation rate could result from (i) absorption of thermal neutrons by thick stainless steel pressurized pipe; and (ii) by achieving high fast neutron flux benefits from the deployment of the rig directly inside the fuel element, thus screening from other thermal neutrons.

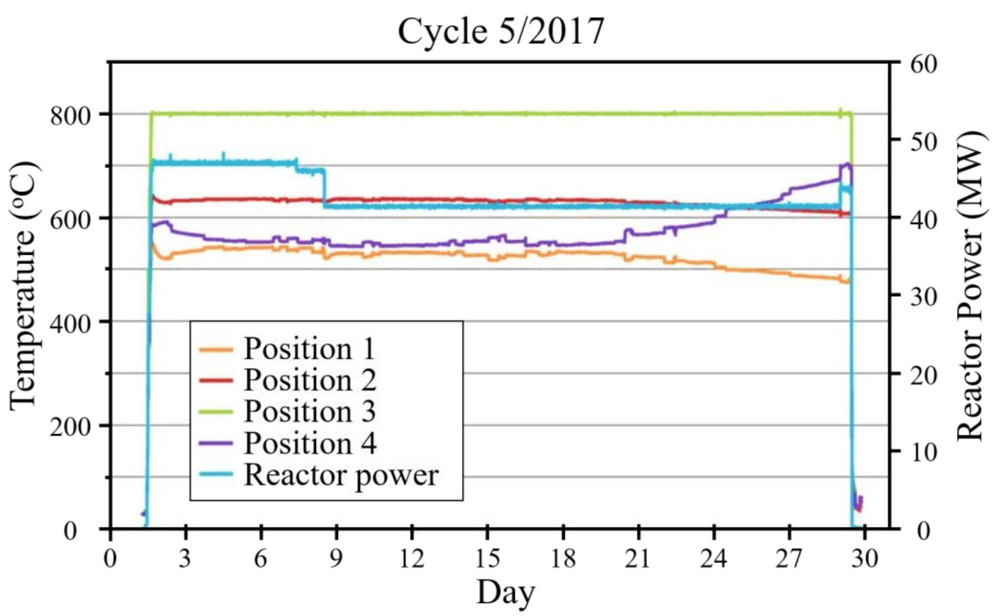

Fig. 2. Evolution of the temperature on the samples located in the T-controlled zone (in green), the temperature on the samples located between T-controlled zone and outer parts of the rig (in red), the temperature on the samples located in the outer parts of the rig (light brown, dark blue), power reactor (in light blue).

2.4. Standard and interrupted tensile tests

Standard uniaxial tensile tests (ST) were performed to determine the load-displacement curve under displacement control. Interrupted uniaxial tensile tests (IT) were implemented to identify the yield strength at various temperatures with a single specimen. This is an original side development of this research. Both standard and interrupted tensile tests are performed in a static tensile mode with a constant crosshead speed of 0.2 mm/min at various temperatures in air. The load is measured by the strain gauge load cell and the displacement is measured by the actuator, which corresponds to the displacement of the crosshead. In order to compensate the machine compliance contribution to the total displacement, the elastic displacement component of each data point from the raw data (u_{tot}) is replaced by the value calculated using the elastic modulus E taken from the literature [35-37]. The equation to account for machine compliance is described as,

$$u = u_{tot} - \frac{F}{K} + \frac{F \cdot L}{E \cdot S} \tag{1}$$

where u is the displacement of the test specimen associated with the gauge length L, F is the load, K is the elastic slope of the raw load-total displacement curve, and S is the area of cross section in the gauge zone. The data corrected for machine compliance are used for the calculation of engineering stress – engineering strain curve and true stress – true strain response of the standard tensile tests.

The development of the interrupted uniaxial tensile test method is driven by the need to determine the temperature dependence of the yield strength using a limited number of specimens available for the tests. The idea of the interrupted tensile test is based on the assumption of a power law relationship between the flow stress and strain (see Appendix A), which prescribes the evolution of the loading rate (N/s). Then, the criterion for the interruption based on the change of the loading rate is proposed and applied to tungsten and steel products. Both products are used to show the conservatism of the proposed approach for materials, which exhibits either a standard stress-strain response or a yield drop (i.e. presence of upper yield strength (UYS)). Complete details of the derivation are provided in Appendix A and B.

Practically, the loading rate is calculated and plotted on the operational screen on the fly during the tensile test. The operator follows the loading rate and stops the pulling displacement once the loading rate reduces to a value lower than half of the maximum loading rate. A typical variation of the load and of its rate with time is shown in Fig. 3a. In order to reduce the noise of the raw *P-t* curve, the experimental data are smoothened using a polynomial function,

$$F = \sum_{x=0}^{9} a_x t^x \tag{2}$$

where F is the load, x is an integer, a_x is a constant, and t is the time. The derivative of the polynomial curve is taken with respect to t. The smoothing process is operated using the Origin analysis software, which only provides one-term to ten-term polynomial. Thus, in order to get the best fit from the software, a ten-term polynomial is implemented. The first derivative of $F(t)$ is the loading rate. The stress at the maximum loading rate (MLR) is defined as σ_E. The stress when the loading rate reduces to half of MLR is defined as the strength at half maximum loading rate (HMLR). The applicability of the HMLR criterion is discussed in Appendix B.

In order to implement the above interrupted tensile test procedure at different temperatures, the heating scheme shown in Fig. 3b is applied. At first, the specimen is heated up to the highest temperature envisaged for the test campaign (around 600 ºC in this study for the irradiated samples). After the first test is performed, the temperature is reduced to the second target temperature to perform another interrupted tensile test and the following steps repeat the same procedure until the test at the lowest target temperature is completed. In order to get the full stress-strain curve of the material at the target temperature, the specimen is heated up again to the target temperature and a standard static tensile test is resumed with the same constant cross-head speed until final fracture. The temperature at each step is maintained for 30 minutes to achieve a homogenous temperature distribution in the specimen and pulling rod before testing.

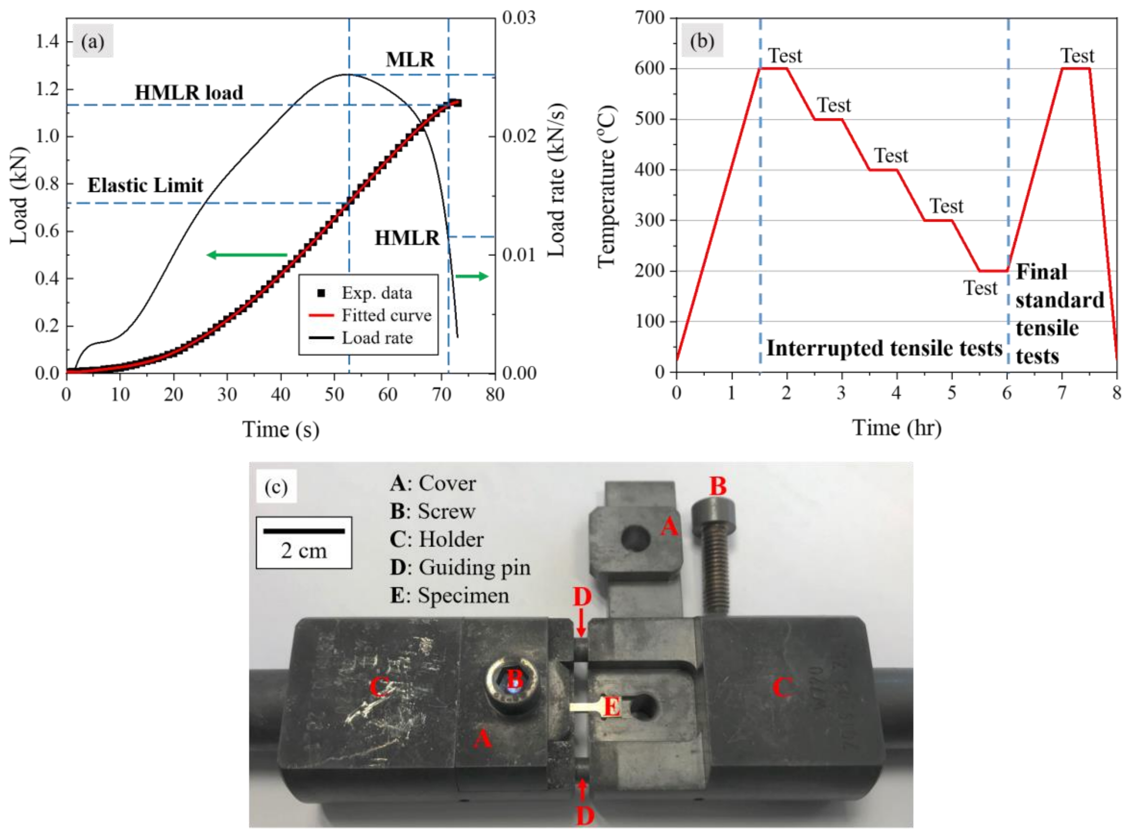

Fig. 3. (a) Variation of the load and loading rate as a function of time for a single temperature test and (b) temperature scheme for the heating process to perform multiple numbers of interrupted tensile tests. (c) set-up of the tensile test holder. Both standard and interrupted tensile tests are uniaxial static tensile test with a constant crosshead speed of 0.2 mm/min. The displacement is measured by the actuator, and the machine compliance is substituted by applying equation (1). Each interrupted tensile test is stopped manually by the operator when the loading rate reduces to a value lower than half of the maximum loading rate. The standard tensile test is stopped after the test specimen is fractured.

To validate the proposed approach, we present the results obtained using both standard and interrupted uniaxial tensile tests for the tungsten products under interest and the Eurofer97 steel. The comparison of the yield stress values extracted from the standard uniaxial tensile tests is provided in Fig. 4. The strength corresponding to the HMLR criterion applied to standard tensile tests has a value close to the 0.2% yield strength (0.2% YS) and UYS at various temperatures for non-irradiated WZrC-L, ATW-L, and Eurofer97. Moreover, HMLR, 0.2% YS, and UYS show similar trends, increasing with decreasing test temperature. The UYS of both tungsten grades and 0.2% YS of ATW-L at 150 °C cannot be found on the plot because the samples fracture before reaching UYS or 0.2% YS, as shown in Fig. 5a–b. A detailed discussion about these results and about the applicability of the interrupted tensile test method in the case of multiple-temperature testing, which involves accumulation of the strain, is provided in Section 3.2.

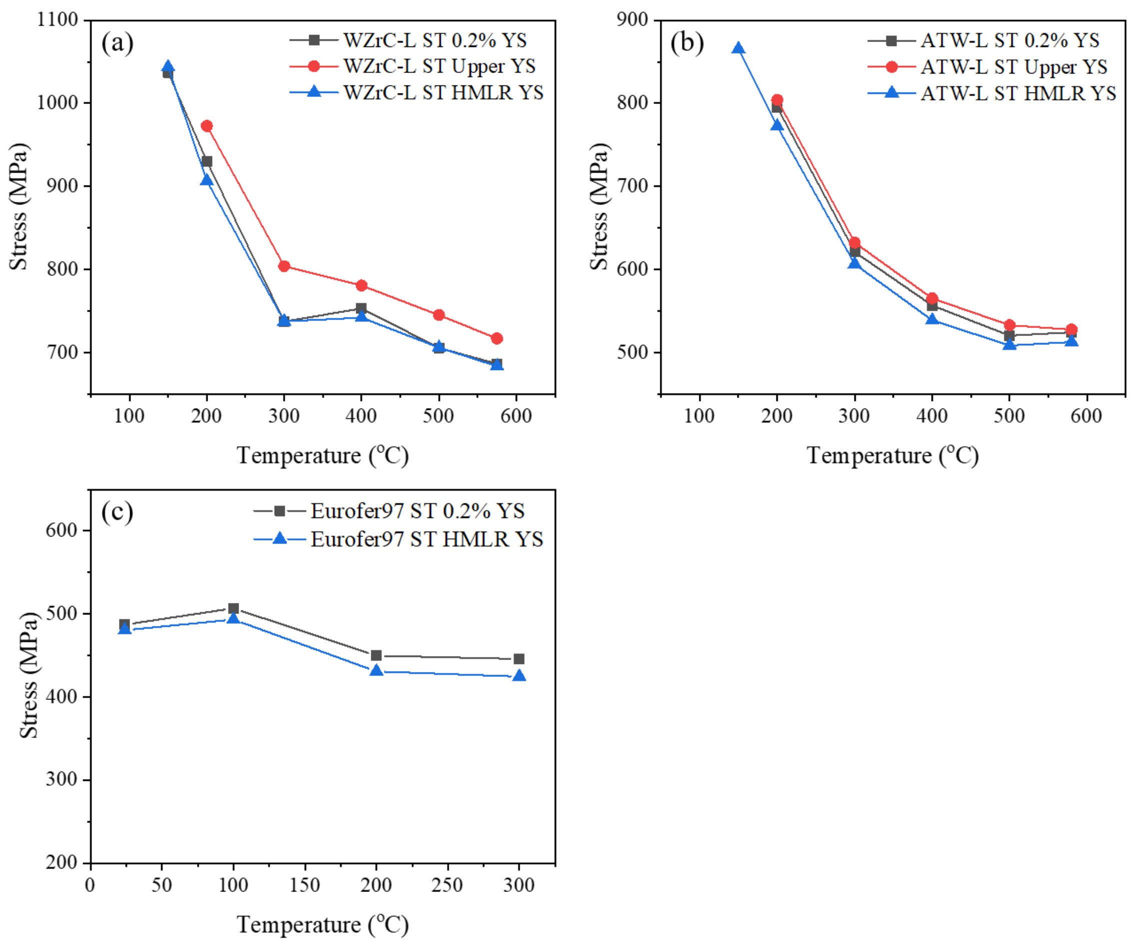

Fig. 4. Comparison of upper yield strength, 0.2% yield strength, and HMLR from the standard uniaxial tensile tests (ST) of WZrC-L (a), ATW-L (b), and Eurofer97 (c) at various temperatures (The data for ATW-L is from our previous work, which can be referred as CEFTR-L [21].)

3. Results and discussion

3.1. Strength and ductility of non-irradiated materials

In order to demonstrate the applicability of the interrupted tensile test procedure, the strength and ductility values of the non-irradiated materials are determined first by standard uniaxial tensile testing. These data are also used for the analysis of HMLR in Appendix B.

The stress-strain curves extracted from the standard uniaxial tensile tests performed at different temperatures (relevant for this study) are shown in Fig. 5. Both tungsten products WZrC-L and ATW-L exhibit an upper yield point at all test temperatures. The Eurofer97 steel does not exhibit the yield drop phenomenon, as shown in Fig. 5c. In WZrC-L and ATW-L materials, a small degree of plastic deformation is attained before reaching the upper yield strength (UYS). This unrecoverable microstrain, a concept introduced in the 1960s [38, 39], is defined as the deformation attained when the stress exceeds σ_E but being lower than UYS. As indicated in the literature [40], the yield drop in tungsten depends on crystallographic orientation. Only the tensile loading along the [110] crystallographic direction involves a yield drop. Moreover, the tensile strength along the [110] crystallographic direction is lower than the one in the [100] direction [22, 40]. Both WZrC-L and ATW-L are deformed during the rolling process. As a result, all the dislocations are free from the interstitial atoms like carbon or nitrogen, which pin these dislocations before deformation. Moreover, more dislocations are emitted after deformation. However, during heat treatment, stress release or tempering, some of the free dislocations are again pinned by the interstitial atoms, which diffuse to dislocations to reduce Gibbs free energy at high temperature. When a tensile test is performed the unpinned dislocations start gliding as the stress reaches the critical resolved shear stress (CRSS) but still within the microstrain region [38, 41]. The mobile dislocation density increases as the pinned dislocations start to be released from the interstitial atoms with increasing stress [39]. Therefore, the larger microstrain before peak found in tungsten might be caused by the combination of strain hardening from unpinned dislocation, release of pinned dislocation, and crystallographic dependence of tensile properties. Because of the larger microstrain before peak, 0.2% yield strength (0.2% YS) can be found before the upper yield strength for both tungsten products.

As shown in Fig. 5a–b, both non-irradiated WZrC-L and ATW-L exhibit only very small plastic deformation at temperature lower than 200 ºC. However, since the small degree of deformation of WZrC-L is larger than the one of ATW-L, the lower boundary of the DBTT range, which was evaluated by tensile property, of WZrC-L should be lower than 150 ºC, presumably around 100 ºC (which is the DBTT reported from a previous study [20]). As a result, the lower boundary of the DBTT range of WZrC-L might be 50 ºC lower than the one for ATW-L, which is around 150 ºC (shown in Fig. 5b).

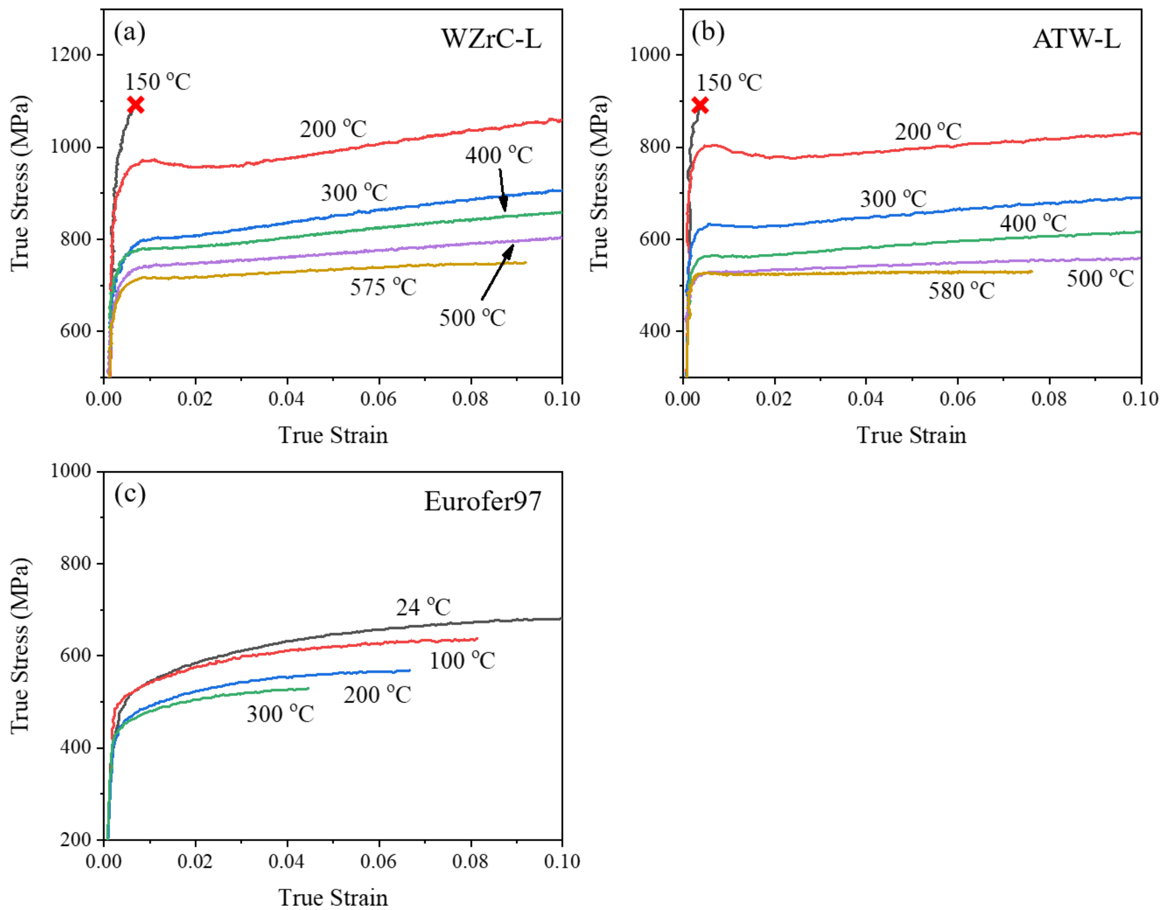

Fig. 5. True stress-strain curves of WZrC-L (a), ATW-L (b), and Eurofer97 (c). The curves here only show data before the ultimate tensile strength. The red cross represents the fracture point. (The data for ATW-L is from our previous work, which can be referred as CEFTR-L [21].)

3.2. Interrupted tensile testing of non-irradiated specimens

An Interrupted Tensile test (IT) is similar to a usual uniaxial tensile test but with loading few cycles of loading/unloading applied at various temperatures. The purpose of the IT is to estimate, from a single specimen, the 0.2% YS or UYS at different temperatures in order to find the variation of the 0.2% YS or of the UYS as a function of temperature. However, in order to identify the yield strength, which indicates the onset of overall plastic deformation, an IT will involve a small plastic strain increment and thus minute amounts of strain hardening after each step. As a result, the strength of the material will slightly increase after each step.

Fig. 6 shows the variation of ΔHMLR and Δ0.2% YS of WZrC-L, ATW-L, and Eurofer97 as a function of temperature. The quantities ΔHMLR and Δ0.2% YS are defined as the change of strength (HMLR or 0.2% YS) at each test temperature with respect to the strength (HMLR or 0.2% YS) at the highest test temperature, in the following way,

$$\Delta HMLR(T) = HMLR(T) - HMLR_{HT} \tag{3}$$

$$\Delta 0.2\%YS(T) = 0.2\%YS(T) - 0.2\%YS_{HT} \tag{4}$$

where $HMLR(T)$ and $0.2\%YS(T)$ is the HMLR and the 0.2%YS at the test temperature T, respectively; the $HMLR_{HT}$ and $0.2\%YS_{HT}$ is the HMLR and the 0.2% YS at the highest test temperature HT, respectively.

Fig. 6 shows that the ΔHMLR extracted from the interrupted tensile tests is regularly higher than the Δ0.2% YS from the standard tests. In the case of ATW product, the mean difference is less than 15 MPa. However, the values of ΔHMLR of WZrC-L and Eurofer97 are higher than Δ0.2 % YS by ~50-100 MPa, and the difference increases with the number of tests (i.e. when approaching lower temperatures). This can be explained by the strain hardening developed within the microstrain regime at each strain achieved before the test is interrupted. Note that Eurofer97 has the highest strain hardening exponent n (0.21 to 0.33, depending on temperature), WZrC-L has the second highest n (0.16 to 0.29), and ATW-L has the lowest n (0.1 to 0.25). Moreover, the magnitude of the plastic strain accumulated after each step will also slightly affect the strain hardening. The plastic strain after each test step is shown in Table 1. Therefore, the material with a higher n and a higher accumulated plastic strain will acquire higher strength step after step. This phenomenon might limit the applicability of IT for materials without a yield drop. Indeed, materials with no softening stage do not exhibit a UYS, which is the basis for indicating the onset of plastic strain after each test step through $R_{L,UYS} = 0$ ($R_{L,UYS}$ is the loading rate ratio of UYS, please refer to Appendix B).

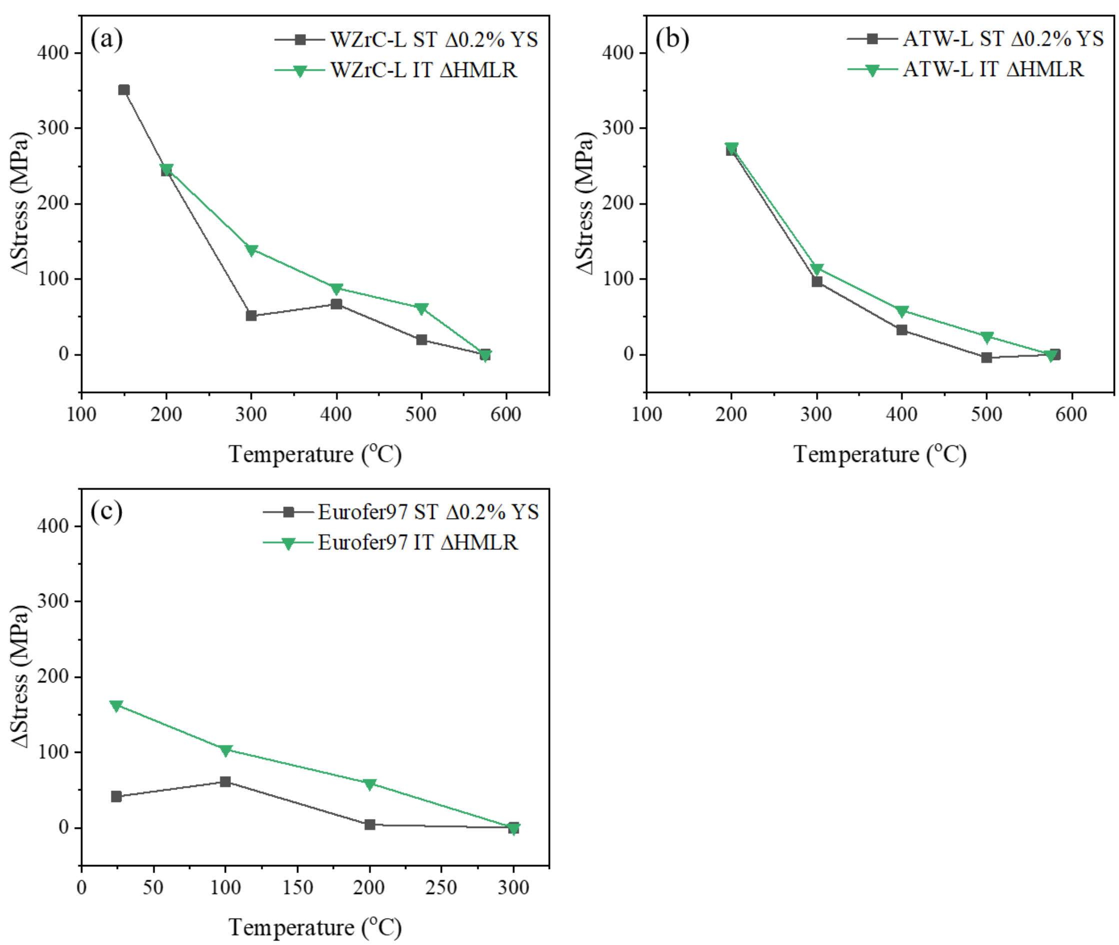

Fig. 6. ΔHMLR from interrupted tensile tests (IT) and Δ0.2% YS from standard tensile tests (ST) of WZrC-L (a), ATW-L (b), and Eurofer97 (c) as a function of temperature (The data for ATW-L ST is from our previous work, which can be referred as CEFTR-L [21].)

Table 1

Plastic strain increment corresponding to each loading step of various test temperatures (T_{test}).

Step #	Plastic Strain (%)					Total Accumulated Plastic Strain[a] (%)
	1	2	3	4	5	
WZrC-L	0.50	0.42	0.43	0.33	0.51	2.19
(T_{test}, ºC)	(575)	(500)	(400)	(300)	(200)	
ATW-L	0.21	0.46	0.35	0.30	0.62	1.94
(T_{test}, ºC)	(575)	(500)	(400)	(300)	(200)	
Eurofer97	1.53	0.37	0.54	0.54	-	2.98
(T_{test}, ºC)	(300)	(200)	(100)	(24)		

[a] The total plastic strain represents the accumulated plastic strain after all test steps from the interrupted tensile test method are finished.

However, if a material exhibits a yield drop, the test will stop before reaching UYS. In other words, the plastic strain after each loading step is smaller than the strain corresponding to UYS. Thus, some of the pinned dislocations are still immobilized at the end of the loading step. Since the pinned dislocations are not all free from interstitial atoms, the yield drop will still happen during each loading step. As a result, the HMLR of an interrupted tensile test will be similar to the UYS of a standard tensile test, as shown in Fig. 7a–b. The HMLR of the first interrupted step is lower than the yield stress derived from the standard test. However, the difference remains well within the spread of 0.2% YS, caused by the natural variation of local microstructure in the material block. Nevertheless, the trend in the HMLR vs. 0.2% YS as a function of temperature for both WZrC-L and ATW-L is well captured by an interrupted tensile test procedure when comparing with standard non-interrupted tests, as shown in Fig. 7c.

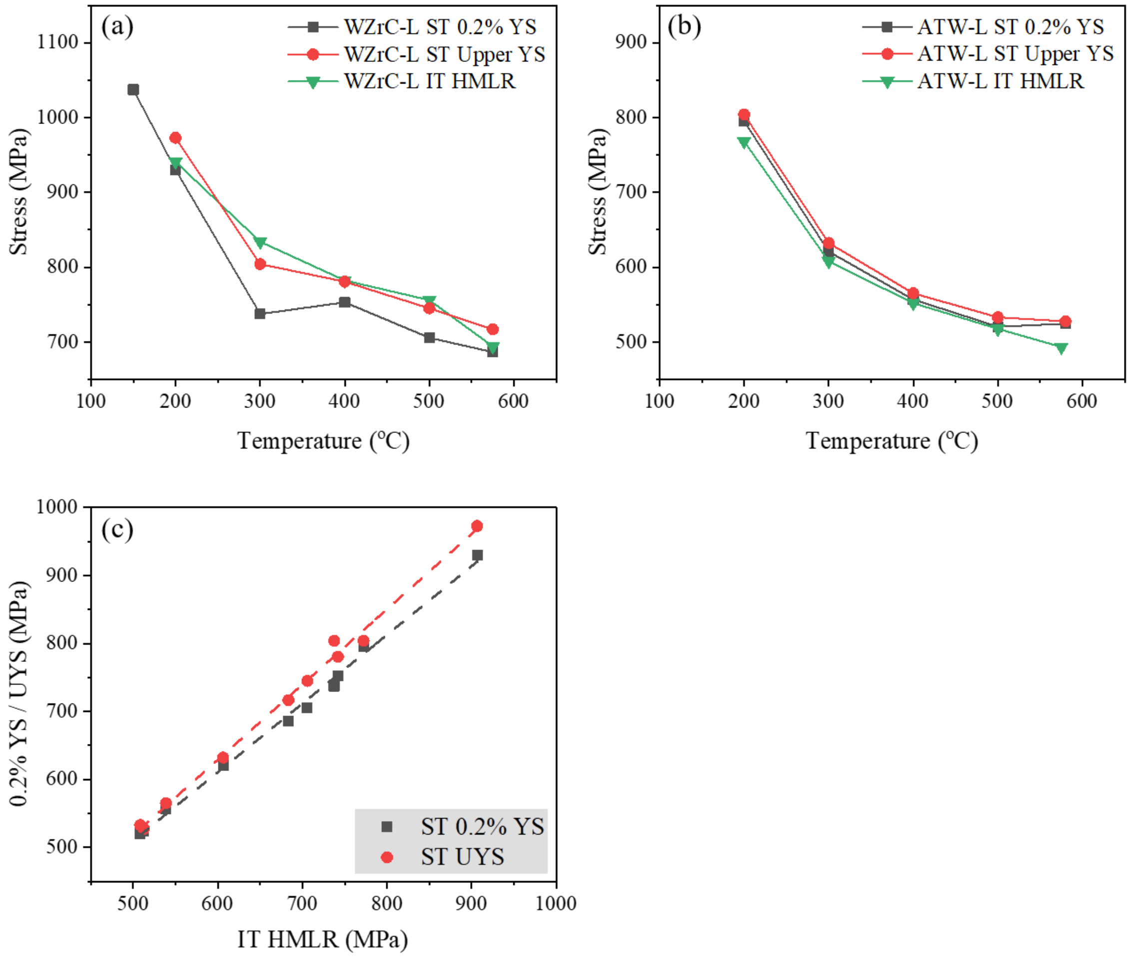

Fig. 7. Comparison of 0.2% YS and UYS from standard tensile tests (ST) with HMLR from interrupted tensile tests (IT). WZrC-L (a), ATW-L (b). (c) Correlation of IT HMLR with ST 0.2% YS and ST UYS for WZrC-L and ATW-L. (The data for ATW-L ST is from our previous work, which can be referred as CEFTR-L [21].)

3.3. Standard and interrupted tensile testing of irradiated samples

Regardless of the irradiation dose and irradiation temperature, the total elongation of both tungsten grades is reduced and the tensile strength is increased by neutron irradiation, as shown in Fig. 8 (detail tensile properties are shown in Table 2). At high temperature (560 – 580 °C), the irradiated WZrC-L shows plastic deformation with almost no strain hardening after UYS for all doses. Unlike WZrC-L, the irradiated ATW-L does not exhibit an UYS but it has a larger strain hardening ability before the deformation reaches ~2.5%. However, as the test temperature drops to 500 °C, the plastic deformation limit of irradiated ATW-L is much smaller compared to the plastic deformation limit of irradiated WZrC-L, which is around 10%. At temperature below 400 °C, no macrostrain (large elongation) is observed in both WZrC-L and ATW-L. Moreover, all irradiated WZrC-L specimens show various degrees of yield drop at test temperatures higher than 500 °C. Neutron irradiation also affects the elongation: the total elongation of all irradiated WZrC-L decreases with increasing irradiation dose and irradiation temperature, as shown in Fig. 8a.

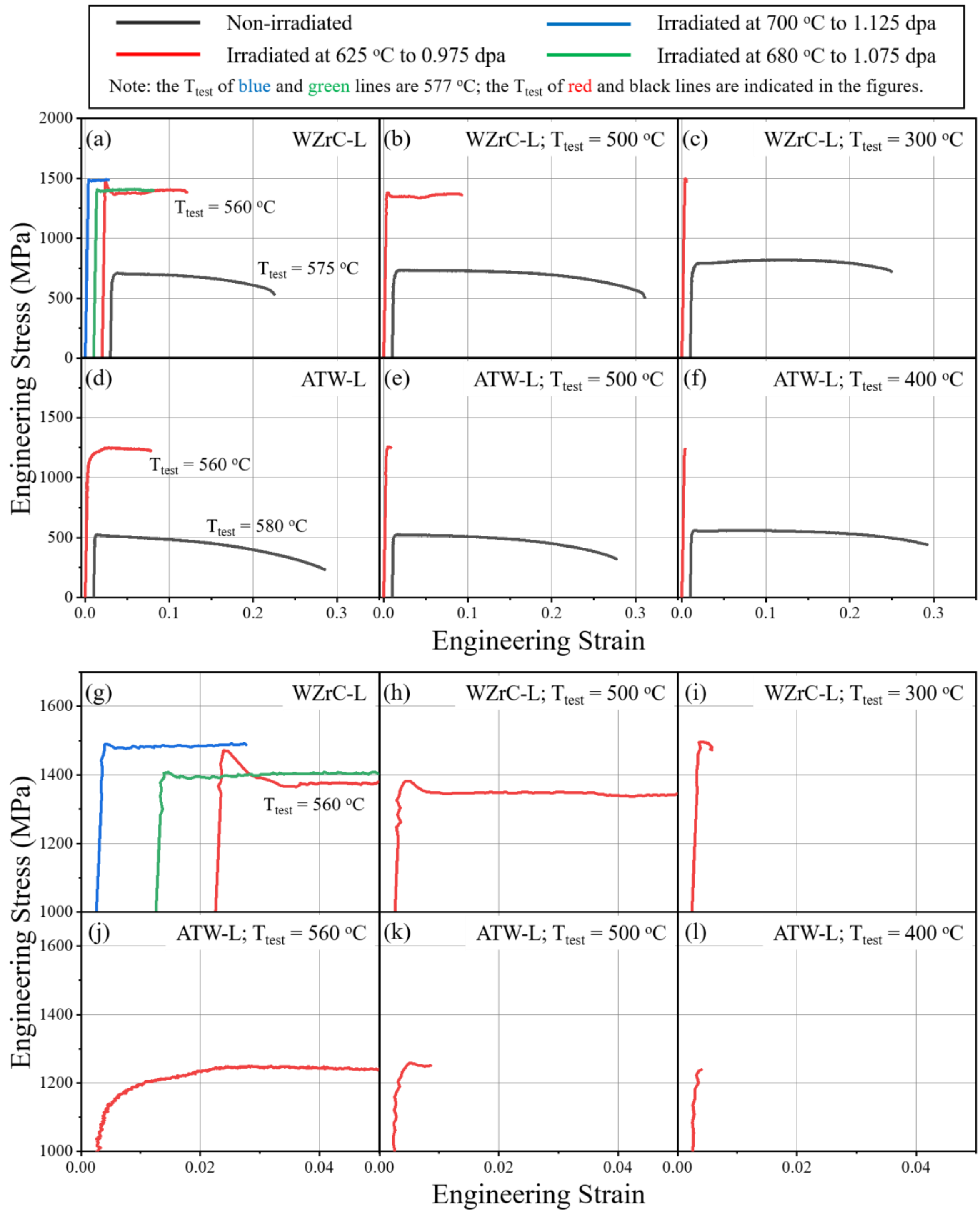

Fig. 8. Engineering stress-strain curves from standard uniaxial tensile tests (ST) of non-irradiated and irradiated samples from WZrC-L (a, b, c) and ATW-L (d, e, f); partial magnification of near yielding region for WZrC-L and ATW-L are shown in (g, h, i) and (j, k, l), respectively. (a, d, g, j) are tested at 560 – 580 °C; (b, e, h, k) are tested at 500 °C; (c, i) are tested at 300 °C; (f, l) are tested at 400 °C. The stress-strain curves are shifted with a strain of 1%. ST of WZrC-L irradiated at 700 °C 1.125 dpa of (a, g), WZrC-L

irradiated at 680 °C 1.075 dpa of (a, g), WZrC-L irradiated at 625 °C 0.975 dpa of (c, i) and ATW-L irradiated at 625 °C 0.975 dpa of (f, l) are performed after interrupted tensile tests. (The data for ATW-L non-irradiated that are tested at 400 and 500 °C is from our previous work, which can be referred as CEFTR-L [21].)

Table 2

Tensile properties of non-irradiated and irradiated WZrC-L and ATW-L.

Materials	Dose (dpa)	Test temperature (°C)	Irrdiation temperature (°C)	0.2% YS (MPa)	UYS (MPa)	UTS (MPa)	Uniform elongation[a] (%)	Total elongation (%)
WZrC-L	0	300	-	737	795	823	10.1	23.8
	0.975	300	625	1493	1497	1497	0.2	0.3
	0	500	-	705	737	737	1.5	30
	0.975	500	625	1384	1388	1388	8.0	9.0
	0	575	-	686	711	711	1.4	19.4
	0.975	560	625	1456	1471	1471	7.4	9.8
	1.075	577	680	1405	1408	1411	4.6	6.8
	1.125	577	700	1347	1490	1492	2.2	2.4
ATW-L[b]	0	400	-	557	561	562	5.9	28.1
	0.975	400	625	-	-	1239	0.1	0.1
	0	500	-	520	525	525	1.6	26.6
	0.975	500	625	1006	1258	1258	0.6	0.6
	0	580	-	524	525	525	0.5	27.4
	0.975	560	625	816	-	1250	2.6	7.6

[a] Uniform elongation is defined as the elongation at which the engineering stress starts to decrease after yield drop.

[b] The data for non-irradiated ATW-L samples tested at 400 and 500 °C is from our previous work, which can be referred as CEFTR-L [21].

The interrupted tensile test method is suitable for irradiated materials since most irradiated materials exhibit a yield drop. The total plastic strain accumulated after the interrupted tensile tests are shown in Table 3. Since irradiated WZrC-L shows a yield drop for all doses and test temperature, the strain hardening effect associated with the accumulated strain during interrupted tensile tests is not a concern. For irradiated ATW-L, as indicated in Fig. 8j, a yield drop is not observed while testing at 560 °C. As mentioned before and shown in Fig. 6, the plastic strain accumulated during the interrupted tensile tests for materials without yield drop needs to be carefully controlled. Therefore, for irradiated ATW-L, the interrupted tensile test for test temperature at 560 °C is not performed and the total plastic strain is maintained within 0.5% or less, as shown in Table 3. Thus, the strain hardening effect is limited in the interrupted tensile testing of irradiated ATW-L and the HMLR approach is applicable to irradiated ATW-L.

Table 3

Total plastic strain after interrupted tensile tests and DBTT range of non-irradiated and irradiated WZrC-L and ATW-L samples.

Materials	Dose (dpa)	Irradiation temperature (^{o}C)	Total accumulated plastic strain (%)	DBTT range (evalued by tensile property, ^{o}C)
WZrC-L	0	-	2.19	100 – 200 [20, 21]
	0.975	625	1.04	300 – 500
	1.075	680	0.73	-
	1.125	700	0.83	-
ATW-L	0	-	1.94	150 – 200 [21]
	0.975	625	0.17	400 – 575

The 0.2% YS, UYS, and HMLR from interrupted tensile tests of all irradiated samples from both tungsten products are around 2 times higher than the HMLR from interrupted tensile tests on non-irradiated samples for both materials at various test temperature, as shown in Fig. 9. Although the UYS and HMLR of all irradiated WZrC-L samples (doses around 1 dpa) scatter, they seem to have similar values (around 1400 MPa) at different temperatures. The lowest temperature at which a microstrain can be detected for WZrC-L irradiated to 0.975 dpa is 300 ^{o}C (Fig. 8i), which is 100 ^{o}C lower than the one of ATW-L irradiated to 0.975 dpa (Fig. 8l). Moreover, this temperature (300 ^{o}C for WZrC-L irradiated to 0.975 dpa, 400 ^{o}C for ATW-L irradiated to 0.975 dpa) is about 200 ^{o}C lower than the threshold to achieve full ductile deformation in WZrC-L and ATW-L (as shown in Fig. 8b and d). Both microstrain and large elongation require mobile dislocation to produce plastic deformation [38, 41]. Therefore, the existence of a microstrain plasticity can be interpreted as a ductile deformation behavior. In other words, the temperature at which microstrain develops prior to UYS can be used as an indication to find the lowest temperature of DBTT range at which the material exhibits some degree of ductility. As a result, the DBTT range, which was evaluated through tensile testing, of WZrC-L is between 300 – 500 ^{o}C and the one of ATW-L is between 400 – 575 ^{o}C after being irradiated to 0.975 dpa at 625 ^{o}C. The DBTT range before and after irradiation for both materials is shown in Table 3.

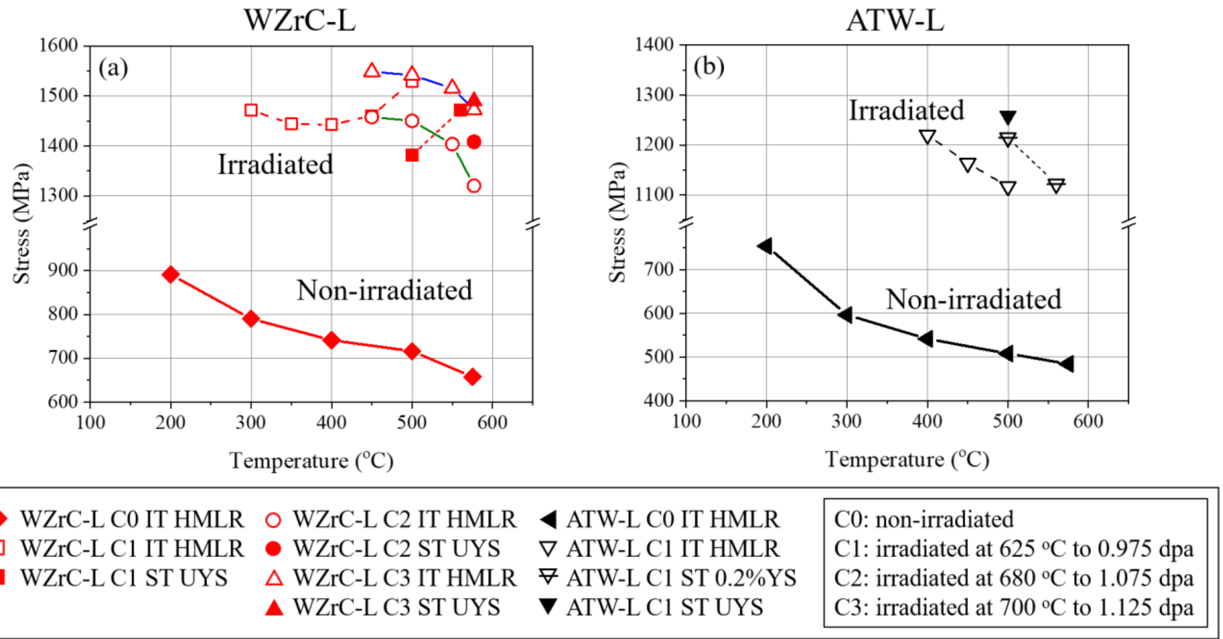

Fig. 9. HMLR from interrupted tensile tests (IT) and 02% YS of all irradiated samples compared to HMLR from IT of non-irradiated samples from WZrC-L (a) and ATW-L (b).

The hardening effect after irradiation increases the strength of both tungsten grades and the strength increments are almost the same. This indicates that both WZrC-L and ATW-L involve a similar strain hardening mechanism. Tungsten, when irradiated by neutrons in the fission reactor, includes more transmutation elements, Re and Os, than if irradiated in a fusion reactor because of the higher fluence of the thermal neutrons, which have a larger cross section for transmutation. As a result, the number of voids or dislocation loops for the materials irradiated in the fission reactor will be smaller since Re suppresses the formation of voids and dislocation loops [42-44].

If the concentration of Re and Os is within the solubility of tungsten, these chemical elements will remain dissolved in the matrix. The effect of Re and Os solid solution on the mechanical properties of W was studied in [45] by hardness tests performed at room temperature. The effect of Re is known to be temperature dependent and strengthening is observed at the temperatures above ~200 °C, while at lower temperatures the softening is observed (given that a certain concentation of Re is attained) [46, 47]. The temperature dependence of strengthening effect of Os is unknown but the hardness tests at room temperature show that it growth proportionally to the Os content [45]. As calculated by MCNP code, the Re and Os concentration after neutron irradiation in this study is within 1.5 at% and 0.2 at%, respectively. Based on the hardness data at elevated temperature provided in [46], the increase of the flow stress due to 1.5 at% of Re is around 3% at 400 °C and 5% at 600 °C. For 0.2 at% of Os, the estimated flow stress increase is around 1% at room temperature [45]. This is clearly a marginal increase of the flow stress compared to the experimentally measured yield stress. However, one needs to keep in mind that the diffusion and segregation of Re and Os is expected in the present experimental conditions, since the irradiation temperature exceeds the one corresponding to the long-range vacancy migration [48], being around 400°C. Thus, the estimates above based on the studies employing solid solution should be carefully analyzed.

After neutron irradiation in HFIR at 700 ^oC for 1 dpa, dislocation loops and voids were observed and precipitates of Re and Os were expected [22, 49, 50]. Although BR2 is a fission reactor, the transmutation rate is lower than in HFIR at the same neutron flux because the irradiation was performed directly inside the fuel element of BR2. Thus, the Re and Os concentration in this study is lower than the one from HFIR irradiation. Therefore, the Re/Os-based precipitates might not form (or might be lower in density and size) in the irradiated WZrC and ATW. Hence, main contribution to the strengthening of WZrC-L and ATW-L after neutron irradiation should be attributed to the dislocation pinning by dislocation loops and voids. The contribution coming from the transmuted Re and Os requires further study employing TEM and atom probe.

To summarize, because irradiation defects will act as obstacles for dislocation gliding in the metal, the critical resolved shear stress increases and the mobility of dislocation, being means of plastic deformation, reduces in the neutron irradiated material. Naturally, with the increase of the flow stress, the DBTT shifts to a higher temperature range. Because the physical nature of the irradiation hardening and DBTT increase is the same (irradiation defects), one can relate the DBTT shift with the increment of the yield strength. This relation between irradiation hardening and shift of DBTT can be perceived from the result of this study where ATW-L and WZrC-L have a similar increment of yield strength and shift of lower boundary of DBTT range (increased temperature is around 200 - 250 ^oC) after irradiated to 0.975 dpa at 625 ^oC.

Since the transmutation rate in the actual fusion reactor environment is lower than in the fission reactors, the strengthening in the plasma-facing tungsten might be lower than the one evaluated in this study at the same irradiation temperature and dose. Moreover, He bubbles are expected to be formed in the sub-surface layer of tungsten operating in a fusion reactor but not in a fission reactor [51]. Therefore, in order to transfer the information related to the neutron irradiation degradation obtained from fission reactor experiments to fusion applications, further study and justifications are required.

Conclusion

Standard and interrupted tensile tests of ITER specification and ZrC reinforced tungsten products have been performed at elevated temperature to assess the impact of neutron irradiation on the flow stress and ductility. Neutron irradiation was performed in BR2 material test reactor with mixed spectrum at 625 ± 25 ^oC up to a dose of ~1 dpa. The obtained results led to the following findings.

Firstly, an interrupted tensile testing approach is proposed and validated. The assumption of determining the strength at half maximum loading rate (HMLR) gives a reliable trend for the upper yield strength (UYS) as a function of temperature. The accuracy for determination of the yield stress is found satisfactory for materials exhibiting the yield drop. For materials without the yield drop, careful control of the magnitude of the plastic strain increment after each step of the interrupted tensile test is required to limit the effect of strain hardening, which results in an overestimation of the yield stress from HMLR.

Secondly, the main results of the irradiation campaign can be summarized as follows:

- The elongation of both WZrC-L and ATW-L products is reduced after the irradiation. Both products remain ductile at the irradiation temperature. However, the DBTT range, which was evaluated through tensile testing, of WZrC (being between 300 – 500 ^oC) is lower than the one of ATW product (being between 400 – 575 ^oC). At the same time, the shift of DBTT, which is around 200 – 250 ^oC, is similar for both materials.
- The hardening effect after the neutron irradiation is similar for both WZrC-L and ATW-L where the strength increases by almost a factor of two for all irradiated specimens. The irradiation

hardening is primarily attributed to dislocation loops and voids, since the transmutation of Re and Os was limited benefits from the irradiation position, which is located inside the fuel element.

Acknowledgments

This work has been carried out within the framework of the EUROfusion Consortium and has received funding from the Euratom research and training programme 2014–2018 and 2019-2020 under grant agreement No. 633053. Additional funding is supported by the National Natural Science Foundation of China under grant No. 51771184. The views and opinions expressed herein do not necessarily reflect those of the European Commission. Moreover, Chao Yin thanks for the help of Dan Chen, and Aleksandr Zinovev. Dmitry Terentyev acknowledges Athina Puype and OCAS for providing the Eurofer97 steel.

Appendix A: Relationship between hardening rate and strain hardening

The true stress-strain response can be defined into two regimes, as shown in Fig. A.1. One is the elastic regime (red line) and the other one corresponds to the plastic regime (blue line). In the elastic regime, the true stress σ is proportional to the elastic strain ε_e with the theoretical elastic modulus E:

$$\sigma = E\varepsilon_e \qquad (\sigma < \sigma_E)\ . \tag{A.1}$$

When σ exceeds the elastic limit σ_E, plastic deformation starts and the strength increases, equal to σ. A typical hardening law in metals is given by Ludwik's equation:

$$\sigma \equiv \sigma_p = K(\varepsilon - \varepsilon_e)^n + E\varepsilon_E \qquad (\sigma \geq \sigma_E) \tag{A.2}$$

where K is a strength coefficient, ε is the true total strain, ε_e is the elastic strain, n is the strain hardening exponent, and ε_E is the strain at the elastic limit.

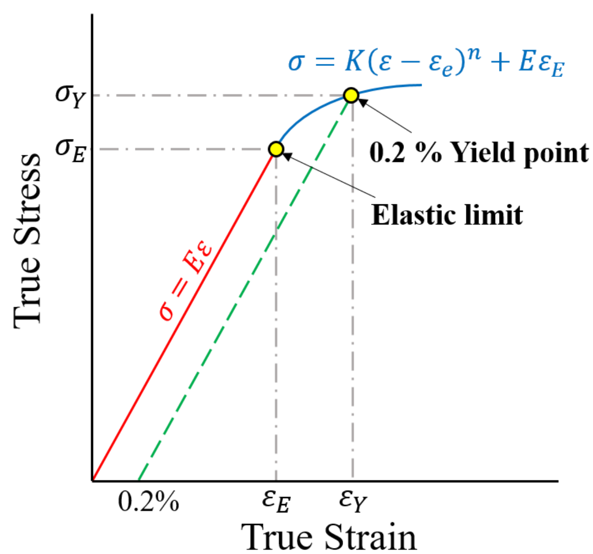

Fig. A.1. True stress-strain curve at early yielding

The hardening rate σ' is defined as the derivative of σ with respect to ε. When σ is larger than the elastic limit σ_E, the relation between σ' and ε is given for the Ludwik's equation, as

$$\frac{d\sigma}{d\varepsilon} = \sigma' = \frac{nKE}{E(\varepsilon-\varepsilon_e)^{1-n}+nK} \ . \tag{A.3}$$

Since the plastic strain ε_p is equal to $\varepsilon - \varepsilon_e$,

$$\frac{d\sigma}{d\varepsilon} = \sigma' = \frac{nKE}{E(\varepsilon_p)^{1-n}+nK} \ . \tag{A.4}$$

The hardening rate ratio R_S between $\dot{\sigma}$ and E is defined as,

$$R_S = \frac{\sigma'}{E} = \frac{n}{\frac{E}{K}(\varepsilon_p)^{1-n}+n} \ . \tag{A.5}$$

At the 0.2% yield point, where $\varepsilon_p = 0.2\%$, R_S is given by,

$$R_{S,0.2\%} = \frac{\sigma'}{E} = \frac{n}{\frac{E}{K}(0.2\%)^{1-n}+n} \ . \tag{A.6}$$

These expressions will be used next to analyze the applicability of the interrupted test approach for deducing the yield strength at various temperatures.

Appendix B: Applicability of Half Max Loading Rate (HMLR) and Interrupted tensile test (IT)

In order to evaluate the applicability of the HMLR approach, an analysis of the hardening rate ratio is proposed. The analysis is based on the true stress and true strain before UYS for WZrC-L and ATW-L and for strain smaller than 1% for Eurofer97 from Fig. 5. The loading rate ratio (R_L) is the ratio between loading rate (F') and the maximum loading rate (MRL), which can relate to the raw elastic slope:

$$R_L = \frac{F'}{MRL} \ . \tag{B.1}$$

Both R_L and R_S are unitless. Fig. B.1a shows the R_L and R_S at 0.2% YS, noted as $R_{L,0.2\%}$ and $R_{S,0.2\%}$, respectively. The largest $R_{L,0.2\%}$ is around 0.5 and $R_{S,0.2\%}$ is not larger than 0.1. Therefore, HMLR ($R_{HMLR} = 0.5$) is a conservative approach to estimate the 0.2% YS because the HMLR will be lower than or similar to 0.2% YS, as shown in Fig. 4. HMLR will also be lower than the UYS since the stress rate ratio of UYS $R_{L,UYS}$ is 0.

The value of $R_{L,0.2\%}$ is much higher than $R_{S,0.2\%}$ because $R_{L,0.2\%}$ includes the machine compliance where the elastic slope is much smaller than the theoretical elastic slope from $R_{S,0.2\%}$. R_S increases with higher elastic modulus and strength coefficient but is not sensitive to the variation of strain hardening exponent when 0.1 < n < 0.4, as shown in Fig. B.1b. Therefore, $R_{S0.2\%}$ is equal to $R_{L0.2\%}$ when the elastic modulus takes into account of machine compliance effects. Moreover, the HMLR is not sensitive to the different type of metals but might need to redefine the value of R_{HMLR} for the different testing machine since the machine compliance varies.

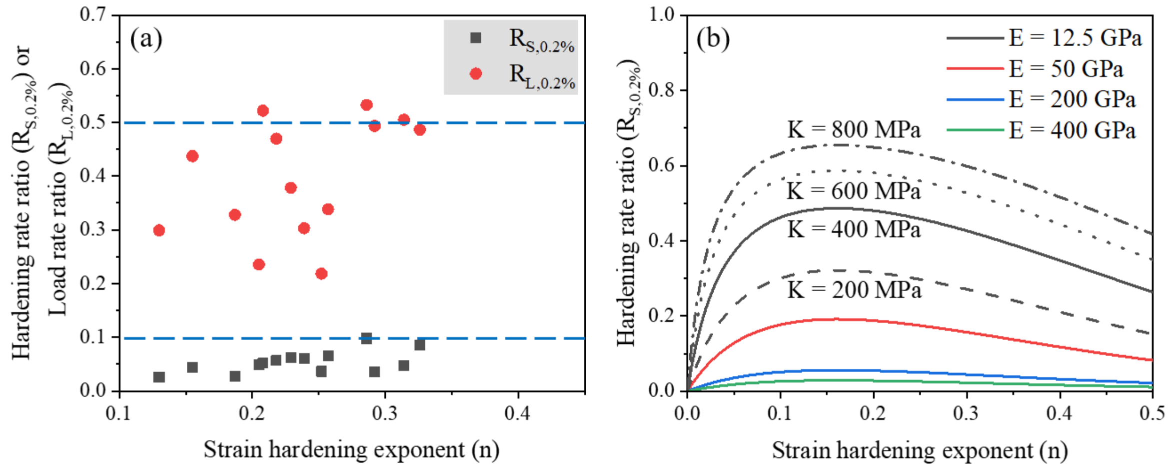

Fig. B.1. Experimental results (a) and theoretical calculation (b) of hardening rate ratio and loading rate ratio at 0.2% yield strength of WZrC-L, ATW-L, and Eurofer97. In (b), solid lines have a K equal to 400 MPa and black lines have a E equal to 12.5 GPa. (The analyzed data includes ATW-L, which is the material “CEFTR-L” from our previous work [21].)

Data availability

The raw/processed data required to reproduce these findings are available by contacting the corresponding author (email: cyin@sckcen.be).

References

[1] D. Maisonnier, I. Cook, S. Pierre, B. Lorenzo, D.P. Luigi, G. Luciano, N. Prachai, P. Aldo, DEMO and fusion power plant conceptual studies in Europe, Fusion Engineering and Design 81(8-14) (2006) 1123-1130.

[2] T.R. Barrett, G. Ellwood, G. Pérez, M. Kovari, M. Fursdon, F. Domptail, S. Kirk, S. McIntosh, S. Roberts, S. Zheng, Progress in the engineering design and assessment of the European DEMO first wall and divertor plasma facing components, Fusion Engineering and Design 109-111 (2016) 917-924.

[3] R. Pitts, X. Bonnin, F. Escourbiac, H. Frerichs, J. Gunn, T. Hirai, A. Kukushkin, E. Kaveeva, M. Miller, D. Moulton, Physics basis for the first ITER tungsten divertor, Nuclear Materials and Energy 20 (2019) 1-25.

[4] J. You, E. Visca, T. Barrett, B. Böswirth, F. Crescenzi, F. Domptail, M. Fursdon, F. Gallay, B. Ghidersa, H. Greuner, European divertor target concepts for DEMO: Design rationales and high heat flux performance, Nuclear Materials and Energy 16 (2018) 1-11.

[5] D. Stork, P. Agostini, J.L. Boutard, D. Buckthorpe, E. Diegele, S.L. Dudarev, C. English, G. Federici, M.R. Gilbert, S. Gonzalez, A. Ibarra, C. Linsmeier, A.L. Puma, G. Marbach, L.W. Packer, B. Raj, M. Rieth, M.Q. Tran, D.J. Ward, S.J. Zinkle, Materials R&D for a timely DEMO: Key findings and recommendations of the EU Roadmap Materials Assessment Group, Fusion Engineering and Design 89(7-8) (2014) 1586-1594.

[6] D. Stork, P. Agostini, J.L. Boutard, D. Buckthorpe, E. Diegele, S.L. Dudarev, C. English, G. Federici, M.R. Gilbert, S. Gonzalez, A. Ibarra, C. Linsmeier, A. Li Puma, G. Marbach, P.F. Morris, L.W. Packer,

B. Raj, M. Rieth, M.Q. Tran, D.J. Ward, S.J. Zinkle, Developing structural, high-heat flux and plasma facing materials for a near-term DEMO fusion power plant: The EU assessment, Journal of Nuclear Materials 455(1-3) (2014) 277-291.
[7] G. Pintsuk, Tungsten as plasma facing material, Comprehensive Nuclear Materials 4 (2012) 551-581.
[8] A. Giannattasio, Z. Yao, E. Tarleton, S.G. Roberts, Brittle–ductile transitions in polycrystalline tungsten, Philosophical Magazine 90 (2010) 3947-3959.
[9] J.M. Steichen, Tensile properties of neutron-irradiated TZM and tungsten, Journal of Nuclear Materials 60(1) (1976) 13-19.
[10] I.V. Gorynin, V.A. Ignatov, V.V. Rybin, S.A. Fabritsiev, V.A. Kazakov, V.P. Chakin, V.A. Tsykanov, V.R. Barabash, Y.G. Prokofyev, Effects of neutron-irradiation on properties of refractory-metals, Journal of Nuclear Materials 191 (1992) 421-425.
[11] I. Alexandrov, I.V. Gorynin, Metallovedenie 22 (1979) 35.
[12] H. Noto, S. Taniguchi, H. Kurishita, S. Matsuo, T. Ukita, K. Tokunaga, A. Kimura, Effect of grain orientation and heat treatment on mechanical properties of pure W, Journal of Nuclear Materials 455(1-3) (2014) 475-479.
[13] H. Sheng, G. Van Oost, E. Zhurkin, D. Terentyev, V.I. Dubinko, I. Uytdenhouwen, J. Vleugels, High temperature strain hardening behavior in double forged and potassium doped tungsten, Journal of Nuclear Materials 444(1-3) (2014) 214-219.
[14] G. Pintsuk, I. Uytdenhouwen, Thermo-mechanical and thermal shock characterization of potassium doped tungsten, International Journal of Refractory Metals and Hard Materials 28(6) (2010) 661-668.
[15] B. Gludovatz, S. Wurster, A. Hoffmann, R. Pippan, Fracture toughness of polycrystalline tungsten alloys, International Journal of Refractory Metals and Hard Materials 28(6) (2010) 674-678.
[16] J. Reiser, S. Wurster, J. Hoffmann, S. Bonk, C. Bonnekoh, D. Kiener, R. Pippan, A. Hoffmann, M. Rieth, Ductilisation of tungsten (W) through cold-rolling: R-curve behaviour, International Journal of Refractory Metals and Hard Materials 58 (2016) 22-33.
[17] S. Wurster, R. Pippan, Miniaturized cantilever bending experiments for determination of fracture properties of tungsten as a model material, 2nd International Conference SSTT: Determination of Mechanical Properties of Materials by Small Punch and Other Miniature Testing Techniques, Ostrava, 2012, pp. 271-275.
[18] J.W. Coenen, S. Antusch, M. Aumann, W. Biel, J. Du, J. Engels, S. Heuer, A. Houben, T. Hoeschen, B. Jasper, F. Koch, J. Linke, A. Litnovsky, Y. Mao, R. Neu, G. Pintsuk, J. Riesch, M. Rasinski, J. Reiser, M. Rieth, A. Terra, B. Unterberg, T. Weber, T. Wegener, J.H. You, C. Linsmeier, Materials for DEMO and reactor applications-boundary conditions and new concepts, Physica Scripta T167 (2016).
[19] M. Rieth, e. al., A brief summary of the progress on the EFDA tungsten materials program, Journal of Nuclear Materials 442(1-3) (2013) S173-S180.
[20] Z.M. Xie, R. Liu, S. Miao, X.D. Yang, T. Zhang, X.P. Wang, Q.F. Fang, C.S. Liu, G.N. Luo, Y.Y. Lian, X. Liu, Extraordinary high ductility/strength of the interface designed bulk W-ZrC alloy plate at relatively low temperature, Scientific Reports 5 (2015) 1-11.
[21] C. Yin, D. Terentyev, T. Pardoen, A. Bakaeva, R. Petrov, S. Antusch, M. Rieth, M. Vilemova, J. Matejicek, T. Zhang, Tensile properties of baseline and advanced tungsten grades for fusion applications, International Journal of Refractory Metals and Hard Materials 75 (2018) 153-162.
[22] L.M. Garrison, Y. Katoh, N.A.P. Kiran Kumar, Mechanical properties of single-crystal tungsten irradiated in a mixed spectrum fission reactor, Journal of Nuclear Materials 518 (2019) 208-225.
[23] M. Rieth, R. Doerner, A. Hasegawa, Y. Ueda, M. Wirtz, Behavior of tungsten under irradiation and plasma interaction, Journal of Nuclear Materials 519 (2019) 334-368.
[24] J. Habainy, Y. Dai, Y. Lee, S. Iyengar, Mechanical properties of tungsten irradiated with high-energy protons and spallation neutrons, Journal of Nuclear Materials 514 (2019) 189-195.
[25] Z.M. Xie, T. Zhang, R. Liu, Q.F. Fang, S. Miao, X.P. Wang, C.S. Liu, Grain growth behavior and mechanical properties of zirconium microalloyed and nano-size zirconium carbide dispersion strengthened tungsten alloys, International Journal of Refractory Metals and Hard Materials 51 (2015) 180-187.

[26] X.D. Yang, Z.M. Xie, S. Miao, R. Liu, W.B. Jiang, T. Zhang, X.P. Wang, Q.F. Fang, C.S. Liu, G.N. Luo, X. Liu, Tungsten-zirconium carbide-rhenium alloys with extraordinary thermal stability, Fusion Engineering and Design 106 (2016) 56-62.
[27] A. Puype, L. Malerba, N. De Wispelaere, R. Petrov, J. Sietsma, Effect of processing on microstructural features and mechanical properties of a reduced activation ferritic/martensitic EUROFER steel grade, Journal of Nuclear Materials 494 (2017) 1-9.
[28] D. Pelowitz, J. Durkee, J. Elson, M. Fensin, M. James, R. Johns, G. McKinney, S. Mashnik, L. Waters, T. Wilcox, MCNPX 2.7. 0 Extensions, Los Alamos National Laboratory, 2011.
[29] S.L. Dudarev, DPA definition and estimates, 2015. https://www-amdis.iaea.org/CRP/IrradiatedTungsten/RCM2/RCM2Presentation-DudarevDPA-2015-09-10.pdf.
[30] A. Stankovskiy, G. Van den Eynde, L. Fiorito, ALEPH V.2.7, A Monte Carlo Burn-Up Code, SCK CEN, 2018.
[31] JEFF Scientific Working group, The joint evaluated fission and fusion nuclear data library, JEFF-3.3, Nuclear Energy Agency, 2017.
[32] D.A. Brown, M. Chadwick, R. Capote, A. Kahler, A. Trkov, M. Herman, A. Sonzogni, Y. Danon, A. Carlson, M. Dunn, ENDF/B-VIII. 0: the 8th major release of the nuclear reaction data library with CIELO-project cross sections, new standards and thermal scattering data, Nuclear Data Sheets 148 (2018) 1-142.
[33] A.Y. Konobeyev, U. Fischer, Y.A. Korovin, S. Simakov, Evaluation of effective threshold displacement energies and other data required for the calculation of advanced atomic displacement cross-sections, Nuclear Energy and Technology 3(3) (2017) 169-175.
[34] M. Norgett, M. Robinson, I. Torrens, A proposed method of calculating displacement dose rates, Nuclear Engineering and Design 33(1) (1975) 50-54.
[35] B. Drapkin, The variation in young's modulus of Fe-Cr, Fe-Mo, and Fe-W alloys, Strength of Materials 5(4) (1973) 475-476.
[36] R. Lowrie, A. Gonas, Single-Crystal Elastic Properties of Tungsten from 24° to 1800° C, Journal of Applied Physics 38(11) (1967) 4505-4509.
[37] Z. Yuan, F. Li, P. Zhang, B. Chen, F. Xue, Mechanical properties study of particles reinforced aluminum matrix composites by micro-indentation experiments, Chinese Journal of Aeronautics 27(2) (2014) 397-406.
[38] J. Meakin, Microstrain behavior of body-centered cubic metals, Canadian Journal of Physics 45(2) (1967) 1121-1134.
[39] R. Kossowsky, N. Brown, Microyielding in iron at low temperatures, Acta Metallurgica 14(2) (1966) 131-139.
[40] A. Argon, S. Maloof, Plastic deformation of tungsten single crystals at low temperatures, Acta Metallurgica 14(11) (1966) 1449-1462.
[41] T. Malis, K. Tangri, Grain boundaries as dislocation sources in the premacroyield strain region, Acta Metallurgica 27(1) (1979) 25-32.
[42] M. Fukuda, N.K. Kumar, T. Koyanagi, L.M. Garrison, L.L. Snead, Y. Katoh, A. Hasegawa, Neutron energy spectrum influence on irradiation hardening and microstructural development of tungsten, Journal of Nuclear Materials 479 (2016) 249-254.
[43] A. Hasegawa, M. Fukuda, K. Yabuuchi, S. Nogami, Neutron irradiation effects on the microstructural development of tungsten and tungsten alloys, Journal of Nuclear Materials 471 (2016) 175-183.
[44] M. Klimenkov, U. Jäntsch, M. Rieth, H. Schneider, D. Armstrong, J. Gibson, S. Roberts, Effect of neutron irradiation on the microstructure of tungsten, Nuclear Materials and Energy 9 (2016) 480-483.
[45] J.-C. He, A. Hasegawa, M. Fujiwara, M. Satou, T. Shishido, K. Abe, Fabrication and characterization of W-Re-Os alloys for studying transmutation effects of W in fusion reactors, Materials Transactions 45(8) (2004) 2657-2660.
[46] E. Savitskii, M. Tylkina, S. Ipatova, E. Pavlova, Properties of tungsten-rhenium alloys, Metal Science & Heat Treatment 2(9) (1960) 483-486.

[47] M. Fukuda, S. Nogami, A. Hasegawa, H. Usami, K. Yabuuchi, T. Muroga, Tensile properties of K-doped W–3% Re, Fusion Engineering and Design 89(7-8) (2014) 1033-1036.
[48] L. Keys, J. Smith, J. Moteff, High-temperature recovery of tungsten after neutron irradiation, Physical Review 176(3) (1968) 851-856.
[49] Y. Katoh, L. Snead, L. Garrison, X. Hu, T. Koyanagi, C. Parish, P. Edmondson, M. Fukuda, T. Hwang, T. Tanaka, Response of unalloyed tungsten to mixed spectrum neutrons, Journal of Nuclear Materials 520 (2019) 193-207.
[50] A. Hasegawa, M. Fukuda, S. Nogami, K. Yabuuchi, Neutron irradiation effects on tungsten materials, Fusion Engineering and Design 89(7-8) (2014) 1568-1572.
[51] J. Marian, T.L. Hoang, Modeling fast neutron irradiation damage accumulation in tungsten, Journal of Nuclear Materials 429(1-3) (2012) 293-297.